Carbohydrate Polymers 87 (2012) 411–421

Contents lists available at ScienceDirect

Carbohydrate Polymers

journal homepage: www.elsevier.com/locate/carbpol

Effect of lignocellulosic filler type and content on the behavior of polycaprolactone based eco-composites for packaging applications

L. Ludueña [a], A. Vázquez [b], V. Alvarez [a,*]

[a] Research Institute of Material Science and Technology (INTEMA), Engineering Faculty, National University of Mar del Plata, Juan B. Justo 4302, (B7608FDQ) Mar del Plata, Argentina
[b] INTECIN (UBA-CONICET), Department of Civil Engineering, Engineering Faculty, University of Buenos Aires, Las Heras 2214, (C1063ACV) Buenos Aires, Argentina

ARTICLE INFO

Article history:
Received 26 May 2011
Received in revised form 5 July 2011
Accepted 31 July 2011
Available online 5 August 2011

Keywords:
Biodegradable polymers
Natural fibers
Mechanical properties
Crystallization
Barrier properties

ABSTRACT

This study was based on the influence of lignocellulosic fillers and content on the morphology, crystallization behavior and thermal, mechanical and barrier properties of fully biodegradable eco-composites based on polycaprolactone for packaging applications. The biodegradation in soil as a function of time was also analyzed. Composites with 5 and 15 wt% of cotton (CO); cellulose (CE) and hydrolyzed-cellulose (HCE) were prepared by melt-mixing. It was determined that, whereas lower content of CO and CE produced a decrease on the crystallinity of the matrix, HCE did not affect it. Increasing the filler content, the crystallinity degree of the matrix decreased at less extent, which was independent on the filler type. A clear reduction on the theoretical melting point, attributed to heterogeneous nucleation sites, took place for the lower content of CO and CE. Induction and half-crystallization times diminished when fillers were incorporated but the effect was less notorious at higher filler contents. All fillers enhanced the Young's modulus of the matrix but the optimal mechanical properties were not obtained with HCE, as was expected, but with CE. After analyzing the main parameters that affect the mechanical properties of the composite; such as morphology, hydrophilicity, crystallinity, mechanical properties and thermal stability of the fillers themselves, interface interaction, filler dispersion and thermal aspects of the composites, we concluded that the parameters responsible for such behavior were the larger aspect ratio, better dispersion and enhanced interface interaction of the CE filler. These parameters also affected the barrier properties and the process of biodegradation in soil of the composites.

1. Introduction

In the last decades the production of biodegradable polymers has attracted increasing attention owing to the environmental problems induced by the accumulation of plastic wastes (Lepoittevin et al., 2002; Petersen et al., 1999). Polycaprolactone (PCL) is a biodegradable and biocompatible polyester that can be processed using conventional plastics machinery (Kunioka, Ninomiya, & Funabashi, 2007; Ludueña, Alvarez, & Vazquez, 2007) and their properties make them suitable for a number of potential applications from agricultural usage to biomedical devices (Dubois, Jacobs, Jerome, & Teyssie, 1991). On the other hand, packaging is the biggest industry of polymer processing but until now, the relative high price and some inferior properties of the PCL have limited their large-scale production as a substitute of traditional polymers (Kim, Kim, & Kim, 2007). Blending PCL with other materials has been proved to be an effective and economic method to overcome this problem (Swapna Joseph et al., 2009; Yu, Dean, & Li, 2006). Natural fibers are an interesting alternative as filler of PCL. They do not only reduce the final price of the material, but also act as reinforcement by increasing the mechanical properties. The main advantages of such fibers are their good mechanical performance, low cost, renewability and biodegradability (El-Tayeb, 2009). Plant fibers are mainly composed of cellulose, hemicellulose and lignin (Akil et al., 2011). Cellulose, which awards the mechanical properties of the complete natural fiber, is ordered in micro-fibrils enclosed by the other two main components: hemicellulose and lignin. Cellulose microfibrils can be found as intertwined micro-fibrils in the cell wall (2–20 μm diameters depending on its source). They are conformed by nano-crystalline domains (width 5–30 nm, length of 20–60 nm) and amorphous regions. A controlled acid hydrolysis can separate both regions driving to crystalline domains with an elastic modulus of 150 GPa (Nishino, 2004). Cellulose is a linear polymer of β-(1 → 4)-D-glucopyranose units. The mechanical properties of natural fibers depend on the type of cellulose. There are several types of cellulose (I, II, III, IV and V), but type I the one that shows better mechanical properties. Hemicellulose is composed of different types of cycled polysaccharides such as xylose, mannose

* Corresponding author. Tel.: +54 223 4816600; fax: +54 223 4810046.
E-mail addresses: luduena@fi.mdp.edu.ar (L. Ludueña), avazquez@fi.uba.ar (A. Vázquez), alvarezvera@fi.mdp.edu.ar (V. Alvarez).

0144-8617/$ – see front matter © 2011 Elsevier Ltd. All rights reserved.
doi:10.1016/j.carbpol.2011.07.064

and glucose, among others. It forms a highly branched random structure. It is mainly amorphous (Nishino, 2004). Lignins are amorphous polymers formed by phenyl-propane units. They mainly consist of aromatic units such as guaiacyl, syringyl and phenyl-propane (Nishino, 2004).

Semi-crystalline thermoplastic polymers have been widely used as matrix of natural fibers reinforced composites (Belgacem & Gandini, 2005; Bledzki & Gassan, 1999; Eichhorn et al., 2001; Freire, Silvestre, Pascoal Neto, Belgacem, & Gandini, 2006; Huda et al., 2005; Oksman, Skrifvars, & Selin, 2003). It is well known that the physical and mechanical properties of semi-crystalline polymers depend on the morphology and the structure of the crystals and on the degree of crystallization (Cyras, Vázquez, & Kenny, 2001; Strawhecker & Manias, 2003). Natural fibers may act as heterogeneous nucleation agents changing the morphology and crystallinity of the interface regions. In the surface of the fibers a high density of nuclei is often observed resulting in a columnar crystalline layer, known as transcrystalline layer (TCL). The TCL ceases to grow when faced with growing spherulites from the bulk (Wang & Liu, 1999). Several parameters affect this process: the nature of the fiber (Gray & Guillet, 1974), the surface roughness of the fiber (Lin, Ding, & Hwang, 2001; Wang & Liu, 1999), the thermal conductivity of the fiber (Cai, Petermann, & Wittich, 1997), the fiber treatment (Son, Lee, & Im, 2000) and the processing conditions (Huson & McGill, 1984; Yue & Cheung, 1993). These parameters can increase or reduce the overall crystallization rate, in most cases depending on the nature of the matrix. Regarding natural fibers, it is not possible to study each factor separately, so, they will act simultaneously and no prediction can be done about the crystallization behavior of the matrix. Despite the importance of the TCL on the performance of the composite, the exact mechanism for the formation of the TCL is still unknown (Quan, Li, Yang, & Huang, 2005).

It can be found in the literature (Nishino, 2004; Chen, Liu, Chang, Cao, & Anderson, 2009; Petersson & Oksman, 2006) that both the Young's modulus and strength of natural fibers show the following increasing tendency: natural fiber < cellulose < partially hydrolyzed cellulose < nano-cellulose domains. For that reason, the chemical treatments used to obtain nano-cellulose from natural fibers to employ them as reinforcement of polymeric matrices, have received growing attention (Nishino, 2004; Chen et al., 2009; Morán, Alvarez, Cyras, & Vázquez, 2008; Petersson & Oksman, 2006). Even so, it cannot be ignored that these treatments increase the cost of the final material, they use hazardous solvents for the health and the environment, and they can modify the morphology and chemical composition of the fibers probably worsening three of the main parameters responsible of the final performance of the composite: the chemical compatibility; the interface interaction between the polymer and the filler; and the aspect ratio of the filler (Ku, Wang, Pattarachaiyakoop, & Trada, 2011). Therefore, when hydrolyzed-cellulose/polymer composites are going to be characterized, the results should be compared with those of composites prepared with the same matrix and by the same processing steps but blending with the cellulose and natural fibers that were chosen as raw materials to prepare the hydrolyzed-cellulose. Several authors have analyzed the effect of natural fibers and cellulose micro-nano-fibrils on the thermal, mechanical and barrier properties of different polymeric matrices, few of them including PCL (Angles & Dufresne, 2001; Azizi Samir et al., 2004; Cyras et al., 2001; Dufresne, Dupeyre, & Vignon, 2000; Lönnberg, Fogelström, Berglund, Malmström, & Hult, 2008; Ma, Yu, & Kennedy, 2005; Orts et al., 2005; Sanchez-Garcia, Gimenez, & Lagaron, 2008; Wollerdorfer & Bader, 1998), but a work that compares the effect of these fillers, obtained from the same source, on the final performance of the composite was not found.

The aim of this work was to prepare cellulose and hydrolyzed-cellulose fillers from the same natural source (cotton) and to produce bio-composites based on polycaprolactone with different filler contents. Special effort will be focused in analyzing the effect of the procedures used to prepare each filler on the main parameters that influence the isothermal crystallization process, the thermal, mechanical and barrier properties; and the biodegradation in soil of the composites. It must be taken into account that these are relevant aspects for packaging applications.

2. Experimental

2.1. Materials

Polycaprolactone (M_n = 80,000, density = 1.2 g/cm^3), supplied by Aldrich, was used as a matrix. The fillers were: agricultural cotton (CO); cellulose obtained from cotton (CE) and hydrolyzed cellulose (HCE). Cotton fibers, which are abundant in Argentine, are mainly composed of cellulose (80–90%), lignin (0.7–1.6%) and hemicellulose (4–6%). Because of its high cellulose content, cellulose extraction from these fibers could be a very efficient process.

Cellulose production: CO fibers were dewaxed by boiling in 2/1 ethanol–toluene liquor to liquor ratio for 2 h. Holocellulose (α-cellulose + hemicellulose) was obtained by boiling dewaxed cotton fibers in 0.7 wt% sodium chlorite solution at pH 4 for 2 h using a 1:50 fiber to liquor ratio. It was then treated with sodium bisulphite solution, followed by filtering, washing and drying at 100 °C till constant weight was reached; CE fibers were obtained by treating holocellulose with 17.5 wt% NaOH solution, filtering, washing and drying at 100 °C until constant weight.

Hydrolyzed cellulose production: HCE fibers were prepared by the acid hydrolysis of the obtained CE. The acid hydrolysis was carried out with sulphuric acid (H_2SO_4; PA; Cicarelli) solution 60 wt% at 45 °C for 30 min under continuous stirring.

Composites preparation: an intensive mixer (Brabender type) was used for the melt mixing of the PCL based composites with 5 and 15 wt% of each filler. The temperature, speed of rotation and mixing time were 100 °C; 150 rpm and 10 min respectively. After mixing, samples were compression molded in a hydraulic press at 100 °C for 10 min using a pressure of 50 kg/cm^2. The compression molded composites were named as 5CO, 5CE, 5HCE, 15CO, 15CE and 15HCE, where the number is the percentage filler content by weight and the letters corresponds to the type of filler.

2.2. Characterization

X-ray diffractometry (XRD): X-ray patterns were obtained from a PW1710 diffractometer equipped with an X-ray generator (λ = 0.154060 nm) in the range of 2θ from 5 to 70° at 1°/min.

Thermogravimetric analysis (TGA): TGA measurements of fillers, matrix and composites were carried out by using a Shimadzu TGA-50. The samples were heated from 25 to 1000 °C at a heating rate of 10 °C/min under nitrogen atmosphere.

Scanning electron microscopy (SEM): The SEM photographs of CO and CE were taken with a scanning electron microscope, JEOL JSM-6460 LV instrument. Diameter and length of at least 100 fibers were measured in order to make a statistical distribution. The surface of cryo-fractured composites was also observed by this technique.

Field emission scanning electron microscopy (FESEM): HCE morphology was analyzed in a field emission scanning electron microscope (FE-SEM), SEIZZ SUPRA-25. Diameter and length of at least 100 fibers were measured in order to make a statistical distribution.

Water vapor absorption: 0.1 g of each type of filler was put into glass containers and dried under vacuum at 105 °C for 24 h. Tests were carried out at 65% RH, the temperature was kept at 20 °C and

the pressure was 1 atm. The water adsorbed was analyzed by Eq. (1):

$$WA(\%) = \frac{(m_t - m_0)}{m_0} \times 100 \quad (1)$$

where m_0 is the initial dried mass and m_t is the final mass at the pre-determined time t.

Crystallization behavior: Isothermal bulk-crystallization measurements were carried out in a PerkinElmer 7 DSC (Differential Scanning Calorimeter) under nitrogen atmosphere. The transcrystallization process was study in an optical microscopy Leica DM LB with a hot stage Linkam THMS 600. Samples were prepared by cutting films into small pieces. These samples were heated from room temperature to 100 °C at 10 °C/min, kept at 100 °C for 10 min and then quickly cooled to the crystallization temperature (43 °C) and maintained for at least 1 h. Polarized light was used to observe the spherulites morphology.

Mechanical properties: Tensile tests were performed in a universal testing machine Instron 4467 at a constant crosshead speed of 50 mm/min. Samples were prepared according to the ASTM D882-91 standard. Before tests, all specimens were preconditioned at 65 RH %. Tests were carried out at room temperature. Four samples of each material were tested.

Water vapor transmission (WVT): was determined by following the ASTM E96-00 recommendations by using the Desiccant Method ($CaCl_2$). The films were preconditioned in a chamber at 68% RH and room temperature until reaching equilibrium conditions (2 days). A fan was used to maintain the air continuously circulated throughout the chamber in order to ensure uniform conditions at all test locations. After that, dehydrated Calcium Chloride ($CaCl_2$) was placed in the low chamber of an acrylic cup sealed by the samples. Thus, the corresponding RHs were 0% inside the cup and 68% in the outside. The RH difference promotes a pressure gradient for the vapor transmission. The weights of the assembled cups were recorded every 12 h for 10 days. Weight versus time was plotted for each sample and fitted by linear regression in order to calculate the slope of the resulting line. Permeability values are reported as *WVP* (g m/Pa s m^2) which is determined as follows:

$$WVP = \frac{\Delta W}{\Delta t} \cdot y \cdot [A \cdot (p_2 - p_1)]^{-1} \quad (2)$$

where $\Delta W/\Delta t$ is the calculated slope (weight of water absorbed by the cup/time interval, g/s); y is the film thickness, A is the exposed area of the film and $p_2 - p_1$ is the vapor pressure difference across the film, which is calculated on the basis of the RH and temperature inside and outside the cup. Three samples of each material were tested in order to ensure the reproducibility of the results.

Indoor soil burial experiments: were carried out as reported by Di Franco, Cyras, Busalmen, Ruseckaite, and Vázquez, (2004). Basically, a series of plastic boxes (30 cm × 15 cm × 10 cm) were used as soil containers. Natural microflora present in soil (Pinocha type) was used as the degrading medium. Several specimens (rectangular shape, 10 mm × 20 mm × 0.3–0.5 mm), of PCL and composites obtained from films, were put into cups made of an aluminum mesh to permit the access of microorganisms and moisture and the easy retrieval of the degraded samples. The specimens into the holders were buried at a depth of 8 cm from the surface in order to ensure the aerobic degradation. The average room temperature was 20 °C and relative humidity was kept around 40% by adding distilled water. Samples were removed from the soil at specific intervals (t), carefully cleansed with distilled water and superficially dried. After that, samples were dried under vacuum at 35 °C until constant weight. The specimens were weighed on an analytical balance in order to determine the average weight loss (%*WL*):

$$WL(\%) = \frac{w_0 - w_t}{w_0} \times 100 \quad (3)$$

where w_0 is the initial mass and w_t is the remaining mass at time = t. All results are the average of two replicates.

3. Results and discussion

3.1. Fibers characterization

3.1.1. Diffractometry characterization (XRD)

In order to analyze the crystallinity of the celluloses, XRD patterns (not shown) can be used. The crystallinity index (I_c) can be determined by using the following equation (Mwaikambo & Ansell, 2002):

$$I_c = \frac{\left(I_{(0\,0\,2)} - I_{(am)}\right)}{I_{(002)}} \times 100 \quad (4)$$

where $I_{(002)}$ is the counter reading at peak intensity at a 2θ angle close to 22° (which is separated into two peaks at 22° and 20° as cellulose is transformed from cellulose I to cellulose II) representing crystalline material and $I_{(am)}$ is the intensity of the peak at 2θ angle close to 18° representing the amorphous part of the material in cellulosic fibers. Table 1 summarizes the I_c values for all fibers. Comparing the results for CO and CE fibers a clear trend can be observed since I_c values increases as the reinforcement size is reduced. It can be attributed to the extraction of hemicellulose (mainly amorphous) in the cotton → cellulose transformation. In the case of HCE fibers even higher value of I_c is expected due to the removal of amorphous regions in the cellulose → hydrolyzed-cellulose preparation but the exact value could not be calculated since the amorphous peak at 18° was not observed. It can be thought that this peak disappeared suggesting that the I_c value was close to 100% but it is not possible for this filler to reach such high value. Therefore, our hypothesis is that the amorphous peak was masked by the more intense and wider $I_{(002)}$ peak at 22°. In such case, the value of $I_{(am)}$ in Eq. (4) can be replaced by the intensity data at 18° even when no peak is observed and the minimum value of I_c for the HCE fibers can be calculated as shown in Table 1.

On the other hand, the crystalline peak of the CE fibers was separated into two peaks which indicate the changes from cellulose I to cellulose II. Oh, Yoo, Shin, and Seo, (2005) found the same result with alkaline treated cellulose fibers when the NaOH concentration in the solution was higher than 15 wt%. The relative quantity of cellulose II with respect to cellulose I was near to 42% $\left(\mathrm{Cel_{II}/Cel_I} = (I_{20})/(I_{20} + I_{22}) \times 100\right)$. In the case of HCE fibers the crystalline peak is also separated into two peaks with relative quantity of cellulose II with respect to cellulose I close to 51%.

Table 1
Characteristics of each fiber: crystallinity index (XRD), peak temperatures (TGA) and dimensions (microscopy).

Fiber	I_c (%)	$T_{peak\ (TGA)}$ (°C)	l_{bp} [a] (μm)	d_{bp} [a] (μm)	l [b] (%)	d [b] (%)	l/d [b] (%)	l/d_{bp} [a]	l/d_{ap} [a]
CO	31	349	3870.00 ± 1280.00	59.40 ± 24.90	↓89	↓14	↓87	65.5	8.5
CE	57	349	1191.30 ± 554.70	9.10 ± 3.00	↓27	↓2	↓25	130.9	98.0
HCE	>44	315	1.78 ± 0.49	0.20 ± 0.08	↓16	↓5	↓12	9.0	7.9

[a] Dimensions before processing (*bp* subscript) and after processing (*ap* subscript).
[b] $P(\%) = \frac{P_{ap} - P_{bp}}{P_{bp}} \times 100$, where P is the analyzed parameter.

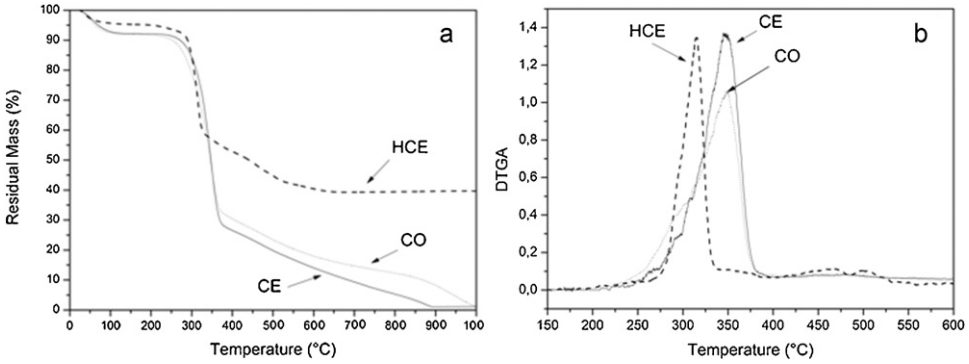

Fig. 1. Thermogravimetrical analysis for CO, CE and HCE: (a) TGA; (b) DTGA.

3.1.2. Thermal stability

Due to the differences in the chemical structure between hemicellulose, cellulose and lignin, they usually decompose at different temperatures. Yang, Yan, Chen, Lee, and Zheng, (2007) showed that cellulose decomposition started at 315 °C and persisted until 400 °C, while the maximum weight loss rate was reached at 355 °C. Hemicellulose started its decomposition at 220 °C and continued up to 315 °C, reaching the maximum mass loss rate at 268 °C. Finally, lignin decomposition extended to the whole temperature range.

The TGA thermograms of each fiber can be seen in Fig. 1(a). The main difference between the different materials is the higher residual content at 1000 °C for HCE fibers. It can be a consequence of the sulfate groups introduced by the hydrolysis with sulfuric acid, which are suspected to act as flame retardants (Roman & Winter, 2004). Fig. 1(b) shows the DTGA analysis and Table 1 resumes the temperatures of the characteristic degradation peaks, T_{peak}, corresponding to the maximum weight loss rate, for each fiber. No difference was found comparing CO and CE may be due to the fact that CO fibers are mainly composed of CE. In the case of HCE fibers, the degradation peak shifted towards lower temperatures indicating lower thermal stability. Same result was found by Wang, Ding, & Cheng (2007). Roman and Winter (2004) reported that the presence of acid sulfate groups would decrease the thermal stability of CE because of the dehydration reaction.

3.1.3. SEM micrographs and analysis of fibers dimensions (before and after melt mixing)

Fig. 2(a–c) shows the SEM micrographs of CO; CE and HCE fibers before melt mixing. CO and CE fibers (Fig. 2(a and b)) exhibited an irregular shape; however, the fibers hydrolyzed from cellulose by sulfuric acid (Fig. 2(c)) were needle-like or rod-like fibers with dimensions close to the nanometer scale. Even so, the diameter of the HCE fibers is higher than that reported in the literature for cellulose whiskers obtained from acid hydrolysis of cellulose (Morán et al., 2008; Morin & Dufresne, 2002). One explanation is that the fibers are partially hydrolyzed but even so it is expected that the mechanical properties of the partially hydrolyzed fibers will be higher than those of cellulose, which was the main motivation of several authors (Azizi Samir, Alloin, & Dufresne, 2005; Dufresne, 2006; Siró & Plackett, 2010), including us, for using them as reinforcement of polymeric materials. In future works we will look for the optimal conditions of the hydrolysis treatment to find the desired morphology of the filler. From these figures, the fibers dimensions (diameter and length) were statistically analyzed before and after processing. In order to carry out the after melt mixing analysis, the fibers were extracted from 5 and 15 wt% composites by the following procedure. The matrix was diluted in tetra-hydrofurane (THF) at room temperature in ultrasonic bath for 5 h. Then, the fiber/diluted-PCL solution was kept at room temperature for 24 h which is enough for filler precipitation. The supernatant THF was extracted and the precipitated filler was dispersed in dymethylformamide at room temperature in ultrasonic bath for 15 min. A droplet of the latter solution was deposited onto a microscopy glass and evaporated in an oven 4 h at 70°. No significant differences were found between the fibers dimensions of 5 and 15 wt% of each fiber/PCL composite. Table 1 also summarizes the average dimensions for each fiber and the geometrical changes of the fibers after processing. Taking into account the CO → CE transformation, the diameter of the filler was more affected than its length, thus the aspect ratio of the CE filler was improved. It can be attributed to the defibrillation of the CO structure seen in Fig. 2(a) as a consequence of lignin and hemicellulose extraction (Rosa et al., 2010). In the case of HCE, both the length and diameter were 100% lower than those of CO, consequently the HCE aspect ratio was dramatically reduced. It can be attributed to amorphous cellulose extraction as was found by Morán et al. (2008). On the other hand, the shear forces developed in the mixer affected more the length than the diameter of the fillers; therefore the aspect ratio (l/d) of the fibers was reduced in all cases. The final result was significant lower aspect ratio for CO (8.5) and HCE (7.9) fibers than that of CE (98.0).

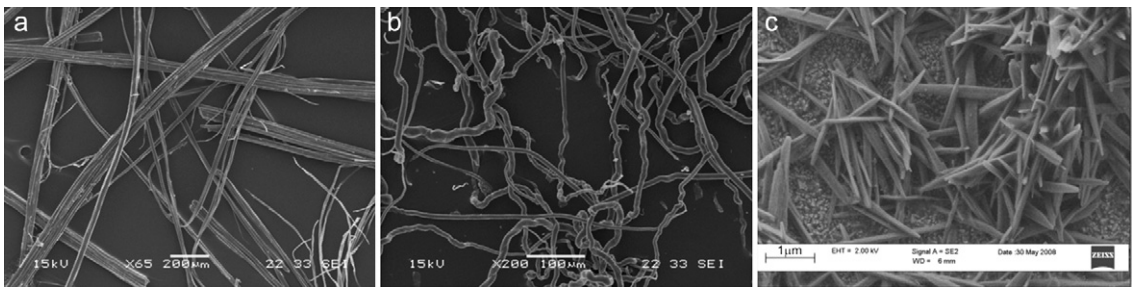

Fig. 2. SEM and FESEM micrographs of the fillers before melt mixing: (a) CO; (b) CE; (c) HCE.

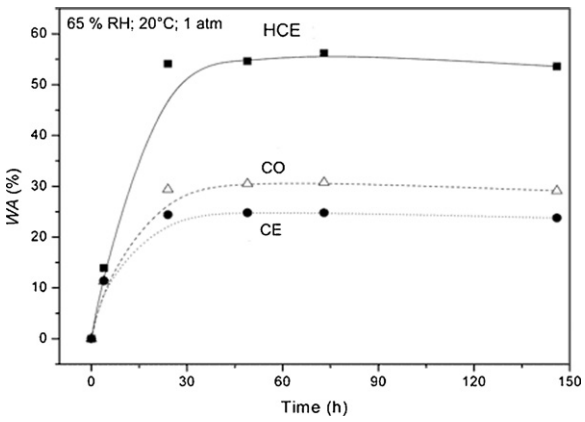

Fig. 3. Water vapor absorption isotherms of CO, CE and HCE as a function of time.

3.1.4. Water vapor absorption

Fig. 3 compares the absorption isotherms of each fiber at 65% RH, 20 °C and 1 atm. It can be seen that all fibers reach the equilibrium at the same time with a moisture content of 24, 29 and 54% for CE, CO and HCE fibers which can be associated to incremented hydrophilicity. The sorption behavior is a combination of two processes: absorption due to micro-cavities and amorphous regions (crystalline regions are considered to be impermeable to vapor molecules) and absorption due to the presence of hydrophilic groups (Bessadok et al., 2009; Gorrasi et al., 2003). The results obtained for CE fibers can be associated to the removal of amorphous components and to the alkaline treatment on holocellulose, which can remove hydrophilic groups as follows:

$$\text{Cotton} \rightarrow \text{Fiber–OH} \rightarrow \text{OH-groups exposed on the surface}$$

$$\text{Cellulose} \rightarrow \text{Fiber–OH} + \text{NaOH} \rightarrow \text{Fiber–O}^{-}\text{Na}^{+} + \text{H}_2\text{O} \rightarrow \text{removal of OH-groups}$$

Amorphous regions of the CE fibers are removed by the acid hydrolysis, thus higher crystallinity is expected for the HCE filler. In this case lower water vapor absorption is expected for HCE but in this work the opposite result was obtained. Belbekhouche et al. (2011) have also reported an unusual water vapor absorption behavior of nanocellulosic films. They observed that the first half-sorption diffusion coefficient corresponding to the diffusion of water through the surface of the nanoparticles was higher than the second half-sorption diffusion coefficient more representative of the diffusion in the core. It is an indication that the diffusion of water is rather controlled by the surface than by the core. In such case, the reduction on the diameter of the HCE filler is also related to an increment on its surface area (cylindrical fibers), which may favor the controlling mechanism for water diffusion inside HCE fibers.

3.2. Composites characterization

3.2.1. Thermal stability

The temperatures of the main degradation peaks for all materials are listed in Table 2. For low filler content (5 wt%), the thermal stability of the matrix was not significantly affected by the presence of the fillers, showing a degradation peak around 415 °C for all analyzed materials. In the case of 15 wt% composites, extra peaks related to the thermal degradation of the fillers (Table 1) were observed. At low filler contents the peaks related to the fillers are not present because the mass of the matrix is substantially higher than that of the fiber, thus equipments with much more sensitivity are needed to reproduce events related to the filler.

3.2.2. Morphology (SEM)

Fig. 4(a–f) shows the surface of cryo-fractured composites. In the case of 5CO and 5CE composites good filler dispersion was observed (Fig. 4(a and c)). The micrograph for 15CO (Fig. 4(b)) shows regions with dispersed fillers and some others with agglomerates while in the 15CE composite the filler remained well-dispersed (Fig. 4(d)). In all these cases filler debonding and pull-out is observed (less extent for CE composites) suggesting weak interfacial strength. Regarding HCE composites, it can be seen large filler agglomerates (Fig. 4(e)) being these effects more notorious for higher filler contents (Fig. 4(f)). The agglomerates do not allow the correct matrix/filler interaction, therefore even weaker polymer/filler interfacial adhesion than for the CO and CE composites is observed, demonstrated by the presence of filler debonding as the failure mechanism. We attribute this result to the high hydrophilicity of the HCE filler (Fig. 3), and hence poor polymer/filler compatibility; and also to the incremented filler exposed surface area that promotes the formation of hydrogen bonds between the individual hydrophilic fibers.

3.2.3. Crystallization behavior

The most relevant parameters used to characterize the crystallization behavior of PCL and composites are shortly described here:

- Degree of crystallinity, X_{cr}:It was calculated by the following equation

$$X_{cr}\,(\%) = \frac{\Delta H_f}{w_{\text{PCL}} \times \Delta H_{100}} \times 100 \tag{5a}$$

  where ΔH_f is the experimental heat of fusion, w_{PCL} is the PCL weight fraction and ΔH_{100} is the heat of fusion of 100% crystalline PCL (136 J/g (Yam, Ismail, Kammer, Schmidt, & Kummerlöwe, 1999)).
- Theoretical melting point, T_m^0:
  It was determined by the Hoffman-Weeks method (Krikorian & Pochan, 2004) through the extrapolation of the experimental points of $T_m = f(T_c)$ to the intercept with the plot of $T_m = T_c$; where T_m is the melting temperature and T_c is the crystallization temperature.
- Induction time, t_i:

Table 2
Characteristics of PCL and composites as a function of filler type and content: thermal degradation and experimental and modeled crystallization parameters.

Material	$T_{peak\ (TGA)}$ (°C)		X_{cr} (%)[a]	T_m^0 (°C)	t_i(s) ΔT = 25 °C	$t_{1/2}$ (s) ΔT = 25 °C	n_{average}	E_a (kJ/mol)
PCL	417		57	66	34	185	2.9 ± 0.3	6.1
5CO	412		39	59	5	11	2.7 ± 0.2	4.4
15CO	355	417	47	67	19	132	3.1 ± 0.1	6.0
5CE	412		41	60	11	13	2.7 ± 0.4	4.3
15CE	354	419	55	67	20	94	3.2 ± 0.1	6.1
5HCE	412		54	65	23	73	3.0 ± 0.2	5.7
15HCE	308	414	49	67	23	82	3.2 ± 0.2	6.0

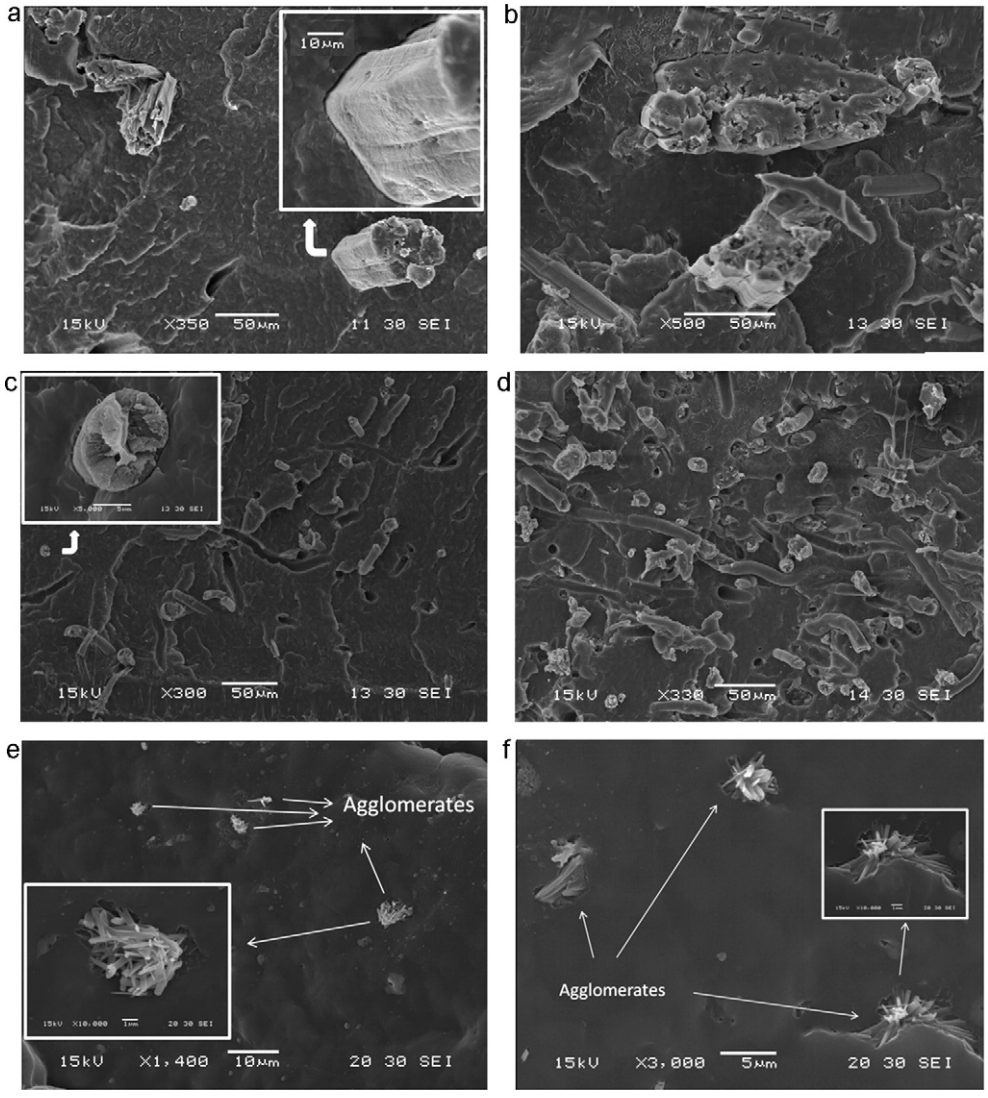

Fig. 4. SEM micrographs of the surface of cryo-fractured composites: (a) 5CO; (b) 15CO; (c) 5CE; (d) 15CE (e) 5HCE; (f) 15HCE.

It is the time at which the first crystal nucleus appears at a given temperature.

- Half-crystallization time, $t_{1/2}$.

It is the time at which the relative degree of crystallinity approaches the value of 0.5. In isothermal crystallization tests the overall crystallization rate is expressed as $(t_{1/2})^{-1}$ (Peneva & Minkova, 2006).

- Avrami's model:

$$\alpha = 1 - \exp\left(-k \cdot t^n\right) \tag{5b}$$

where α is the relative degree of crystallinity at time t, k is the Avrami rate constant (containing the nucleation and the growth parameters) and n is the Avrami exponent (which depends on the nucleation mechanism and the geometry of crystal growth) (Avrami, 1939).

- Arrhenius's equation:

$$k = k_0 \cdot \exp\left(-\frac{E_a}{R \cdot (T_m^0 - T_c)}\right) \tag{5c}$$

where k_0 is a pre-exponential factor, R is the universal gas constant, E_a is the total activation energy (Wu & Liu, 2005).

The experimental and modeled crystallization parameters are summarized in Table 2. In the case of CO and CE composites we can observe that the crystallinity degree, X_{cr}, the theoretical melting point, T_m^0, the induction time, t_i, and the half crystallization time, $t_{1/2}$, of the matrix decreased when 5 wt% of these fillers was added. On the other hand, the increment of the filler content (15 wt%), made this effect less notorious obtaining, in some cases, similar values to that of the neat PCL. Regarding polymer/natural-fiber composites, heterogeneous nucleation on the filler surfaces may be the main mechanism responsible of the crystallization behavior of the matrix. In such case, a high density of nuclei along the interface hinder the lateral extension and force spherulities to growth in one direction, perpendicularly to the filler surfaces, and result in a columnar layer, known as transcrystalline layers; but depending on the filler nature and content, transcrystallization may be restricted by filler–filler contacts and agglomeration which reduce the filler exposed surface area (Cai et al., 1997; Gray & Guillet, 1974; Huson & McGill, 1984; Lin et al., 2001; Quan et al., 2005; Son et al., 2000; Wang & Liu, 1999; Yue & Cheung, 1993). Therefore, the values of X_{cr}, T_m^0, t_i, and $t_{1/2}$ can increase or diminish with respect to the neat matrix depending on the nucleation ability of the filler and the filler content (Hablot, Matadi, Ahzi, & Avérous, 2010; Joseph et al., 2003; Morin & Dufresne, 2002; Pérez, Alvarez,

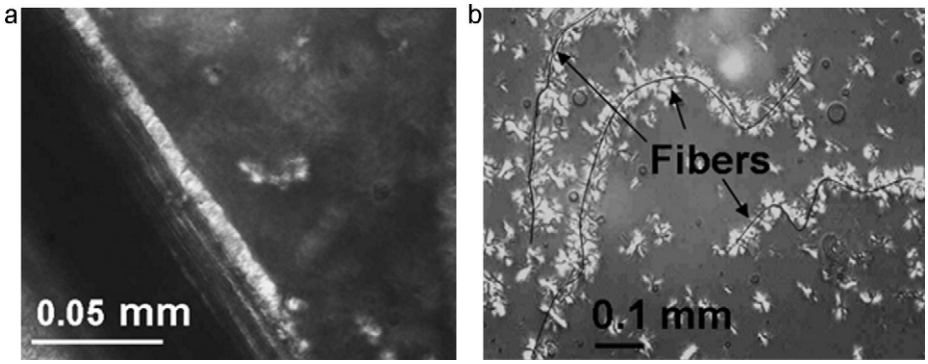

Fig. 5. Optical microscopy showing transcrystalline layers on fibers: (a) CO; (b) CE. Pictures were taken at the end of 4 min of isothermal crystallization at $T_c - T_m^0 = 20\,^{\circ}C$.

Stefani, & Vázquez, 2007). Transcrystallization may reduce the final crystallinity degree of the matrix due to the reduced mobility of polymer chains as a consequence of the fast formation of high density nuclei on the filler surface. This phenomenon also reduces t_i and it can be expected to have the same effect on $t_{1/2}$, since the latter parameter is proportional to both the primary nucleation rate and the crystal/spherulite growth. Heterogeneous nucleation can also reduce the perfection of matrix crystallites lowering T_m^0 (Pérez et al., 2007). Fig. 5 shows that transcrystallinity is present on CO (Fig. 5(a)) and CE (Fig. 5(b)) fillers. It could not be seen on HCE since it requires high resolution with controlled heating and cooling system. The slight differences on X_{cr}, T_m^0, t_i, and $t_{1/2}$ between 5CO and 5CE composites suggests that the sum of the variables that have simultaneous effect on the transcrystallinity (this process is favored by high filler surface–volume relation and surface roughness, low strength and stiffness of the filler, high contents of lignin and hemicellulose and good matrix–filler chemical compatibility (Quan et al., 2005)) is similar for both. Increasing the filler content, the nucleation is hindered as was previously explained and the values of X_{cr}, T_m^0, t_i, and $t_{1/2}$ increase up to values close to those of the neat matrix. In the case of HCE composites, heterogeneous nucleation occurs but the effect is less notorious than for CO and CE composites due to the agglomeration of the filler shown in Fig. 4(e and f). The 15HCE composite showed similar results than that of 5HCE. This result is attributed to the fact that at higher filler content agglomeration can be balanced by the increased volume fraction of the filler, so that the exposed surface area of the reinforcement inside 15HCE composites may be similar than that of 5HCE.

The average n value of the Avrami model and the activation energy E_a for the matrix and all materials are shown in Table 2. The Avrami exponent, n, was around 3 for all materials. In the ideal case, $n = 3$ indicates spherical growth while $n = 2$ indicates circular disk shape growth (Reinsch & Rebenfeld, 1994; Desio & Rebenfeld, 1992). In addition, E_a exhibited the same trend as t_i, and $t_{1/2}$ values as a function of filler type and content. E_a is the total activation energy which consists of the transport activation energy, E^*, and the nucleation activation energy, E_f (E^* refers to the activation energy required to transport molecular segments across the phase boundary to the crystallization surface and E_f is the free energy of formation of the critical size crystal nuclei at T_c) (Wu and Liu, 2005), therefore, it is expected that E_a will be strongly influenced by transcrystallization and, consequently, it is also expected good correlation with t_i, and $t_{1/2}$ values.

3.2.4. Mechanical properties

Table 3 resumes the mechanical properties of the composites and the neat matrix and Fig. 6 shows the relative Young's modulus (E_c/E_m) for each composite as a function of filler content. It is clear that the incorporation of any filler drive to a decrease on the tensile strength (σ) and the elongation at break (ε) as well as an increase on the Young's modulus (E). The best combination of these three parameters was obtained with the 15CE composite. It would be expected to obtain composites with higher stiffness and strength by using HCE as reinforcement (Chen et al., 2009; Petersson & Oksman, 2006) but stiffness is related to several factors such as, the surface roughness (mechanical anchorage), the properties of each phase, the filler aspect ratio, the matrix/filler interfacial strength and the dispersion of the filler inside the matrix. The probability of mechanical interlocking between the filler surface and polymer chains is related to the reinforcement surface roughness but no differences were observed on this parameter (Fig. 2(a and c)). On the other hand, it is expected higher Young's modulus as the reinforcement scale is lower (the highest for HCE and the lowest for CO), which is not only related to the size and perfection of the filler but also to the presence of other components (Nishino, 2004; Brahim & Cheikh, 2007). The same trend is expected for the strength of these fillers. Values reported in the literature are 5.5–12.6 GPa, 30–80 GPa and up to 150 GPa for the Young's modulus of CO, CE and HCE respectively, and 0.5 GPa, 1.7 GPa and 20 GPa for their strength (Nishino, 2004; Brahim & Cheikh, 2007). Furthermore, the crystallinity degree of the matrix in HCE composites was the highest. Therefore it is expected higher Young's modulus and higher tensile strength for the HCE composites but in this work their rigidity and strength were even lower than those of CO composites. The main parameters responsible of this result can be the matrix/filler interfacial strength, the dispersion of the filler inside the matrix and the aspect ratio of the reinforcement (l/d). The first two parameters are strongly dependent on the polymer/filler chemical compatibility

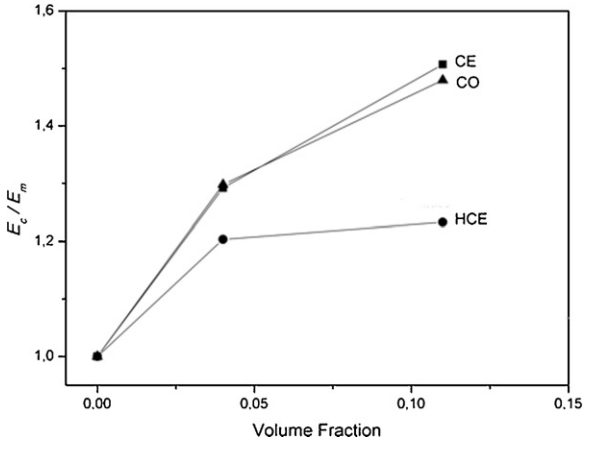

Fig. 6. Relative Young's modulus of the composites as a function of filler content.

Table 3
Mechanical and barrier properties for the neat PCL and their composites.

Material	E (MPa)	σ (MPa)	ε (%)	WVP (g m/Pa s m^2) $\times 10^{-11}$
PCL	330 ± 12	19.0 ± 0.5	897 ± 48	1.6 ± 0.1
5CO	428 ± 46	16.2 ± 0.3	65 ± 13	2.0 ± 0.1
15CO	488 ± 22	14.2 ± 0.3	188 ± 80	2.3 ± 0.1
5CE	426 ± 21	19.0 ± 0.7	572 ± 170	1.6 ± 0.1
15CE	497 ± 40	19.4 ± 0.9	410 ± 65	1.7 ± 0.2
5HCE	396 ± 22	17.6 ± 0.5	707 ± 41	1.9 ± 0.2
15HCE	407 ± 23	12.1 ± 0.7	385 ± 72	2.0 ± 0.4

while the dispersion of the reinforcement may also be dependent on the filler content.

The chemical compatibility between the matrix and the fillers was analyzed from the experimental data of the water vapor absorption tests (see Section 3.1 and Fig. 3). It was previously demonstrated that the trend for the hydrophilicity of the fillers was as follows: CE < CO < HCE which can be associated to the opposite trend for the chemical compatibility with the PCL, which is strongly hydrophobic. In such case it can be observed that polymer/filler chemical compatibility followed the same trend as mechanical properties: the highest for CE composites and the lowest for HCE. A possible reason can be attributed to the fact that the chemical compatibility between the components is intimately related to the interfacial strength. The values of this parameter were not experimentally analyzed in this work and not much works have been reported on the interfacial characterization of natural fiber reinforced thermoplastic composites (Beckermann & Pickering, 2009). Even so, the main failure mechanism for HCE composites was filler debonding (Fig. 4) while CE composites showed pull out and filler debonding but at less extent which suggests stronger interfacial strength. It must be noted that it was the same tendency as that for the chemical compatibility. On the other hand, the interfacial strength is not the only parameter controlling the mechanical properties of the composites. Therefore, other parameters have to be also analyzed to explain the observed tendencies.

The filler dispersion inside the matrix was previously analyzed. It was demonstrated in Fig. 4 higher filler dispersion for CE composites while large agglomerates was observed for HCE composites, also according to mechanical properties results. Fig. 6 shows that in all cases the linearity of E_c/E_m as a function of the filler content is lost at 15 wt% filler content, which suggests that agglomeration of the fillers takes place. This result was more evident for HCE composites accordingly with the previous analysis.

The morphology of the filler is another parameter to be analyzed. After processing, the highest l/d value was obtained with the CE filler. There exist a critical aspect ratio value $(l/d)_c$ below which the matrix–filler load transfer is not efficient. It can be approximated by the Kelly–Tyson equation (de Morais, 2006):

$$\left(\frac{l}{d}\right)_c = \frac{\sigma_f}{2 \cdot \tau_c} \tag{6}$$

where σ_f is the filler strength (extracted from literature (Nishino, 2004)) and τ_c the filler/matrix interfacial strength. τ_c can be replaced by the following expression:

$$\tau_c = \frac{\sigma_m}{2} \tag{7}$$

where σ_m is the matrix tensile strength. The $(l/d)_c$ values were 9.3, 31.5 and 370.4 for CO, CE and HCE composites respectively while their experimental (l/d) values after melt mixing were 8.5, 98.0 and 7.9 respectively. The HCE aspect ratio (after melt mixing) shows the major difference related to its $(l/d)_c$ followed by CO. The same trend was found with the mechanical properties of the composites.

We concluded that the observed tendencies related to the mechanical properties of the composites were a consequence of the combination of the above analyzed parameters: "the highest and lowest chemical compatibility, interfacial strength, filler dispersion and filler aspect ratio were observed for CE and HCE composites respectively", and this was the reason why the expected mechanical behavior (highest mechanical performance for HCE composites) was not observed.

Regarding the tensile strength of the composites, not only the expected results about the effect of the filler type were not observed, but also the composites showed even lower values than that of the neat matrix. Several authors have obtained similar results for natural fiber/polymer composites (Bourmaud & Pimbert, 2008; Singh, Mohanty, Sugie, Takai, & Hamada, 2008) but there have been few attempts to explain the reasons. Beckermann and Pickering (2009) experimentally analyzed the filler strength, the interfacial strength and the critical aspect ratio of the fibers for hemp-fiber reinforced polypropylene composites. Then, they predicted the strength of the composites by means of the Kelly–Tyson modified rule of mixtures (Beckermann & Pickering, 2009) showing that almost no reinforcement effect is observed when the aspect ratio of the filler is ten times lower than its critical value. It must be taken into account that this model assumes no filler–matrix debonding, no voids in the composite and that the properties of the matrix in the composite are the same as those of the neat matrix; therefore the predicted values of the model may be conservative. Furthermore, the critical aspect ratio of the HCE calculated in this work was almost 100 times lower than its critical one, thus finally it is not unexpected to obtain similar or lower strength with the composites reinforced with HCE.

3.2.5. Water vapor permeability

Table 3 shows the WVP (Eq. (2)) values for PCL and composites. It can be seen that while CO and HCE composites have higher values of WVP than the neat matrix, CE composites do not affect it. The balance between the three main mechanisms for water vapor transmission can be responsible for these results (Sanchez-Garcia et al., 2008):

(1) The crystallinity degree of the matrix goes down by the presence of the filler; therefore, the matrix is more permeable to water molecules.
(2) The presence of the filler increases the tortuosity of the pathway for water molecules to pass throughout the sample.
(3) Weak interfacial strength and agglomeration of the filler promotes the generation of voids in the polymer/filler interface making easier the transport of the water molecules throughout these regions.

The highest interfacial strength and dispersion of the filler was observed for CE composites, while the crystallinity of the matrix was the lowest one. The HCE filler did not substantially affect the crystallinity of the matrix but their composites showed the weakest interfacial strength and the highest degree of agglomeration of the filler. On the other hand, CO composites showed intermediate behavior for these phenomena. In all cases the WVP values increase as a function of the filler content, which can be attributed

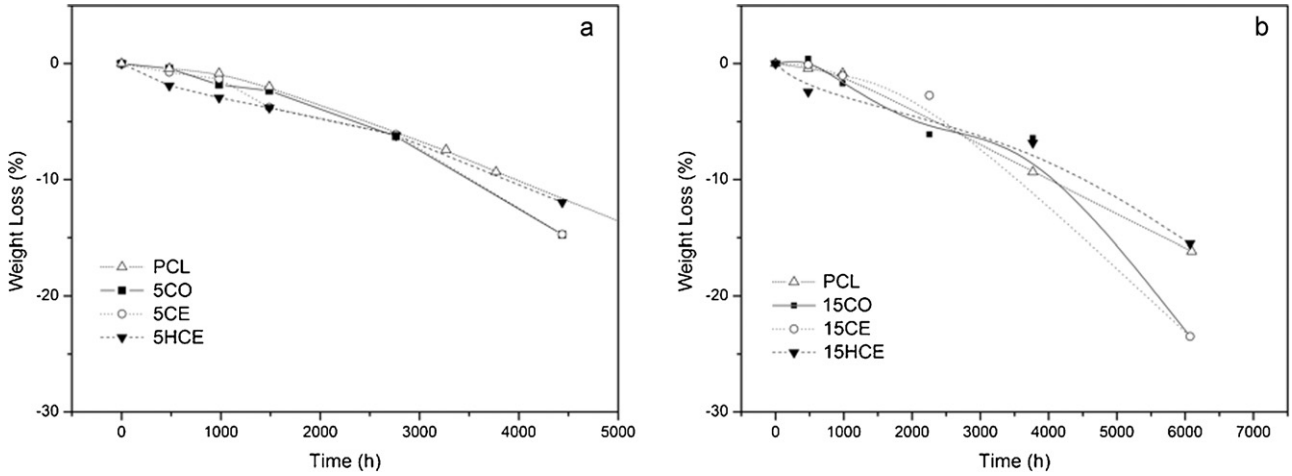

Fig. 7. Biodegradation in soil, weight loss as a function of time for: (a) PCL and their 5 wt% composites; (b) PCL and their 15 wt% composites.

to agglomeration. Similar results for PCL/cellulose composites were obtained by Sanchez-Garcia et al. (2008).

3.2.6. Biodegradation in soil

Fig. 7(a and b) shows the evolution of the weight loss (*WL*) as a function of time for the neat matrix and their composites buried in soil. It can be noted that the data collection was interrupt after the sixth month of testing for the 5 wt% composites and after the ninth month of testing for the neat matrix and their 15 wt% composites. The reason lies on the fact that some fragments of the samples were separated from the specimens by the action of the advanced process of biodegradation and they could not be recovered for weighing.

From Fig. 7(a), it can be observed that after 4400 h of soil-burial the 5CO and 5CE eco-composites show lower weight loss than the neat matrix and 5HCE. This effect is even more notorious increasing the filler content as can be seen after 6000 h of soil-burial in Fig. 7(b). Assuming that the main mechanism for chain scission during the biodegradation in soil of the PCL is the chemical and biological hydrolysis (Grima, Bellon-Maurel, Feuilloley, & Silvestre, 2000), the biodegradation process will be dependent on the water bio-availability that promote the microbial attack and the hydrolysis of the matrix, therefore, the mechanisms for which the water uptake is favored or not are crucial to understand this phenomenon (Alvarez, Ruseckaite, & Vázquez, 2006; Guzman, Gnutek, & Janik, 2011; Zhao et al., 2008). The following characteristics of the fibers themselves and their effect on the properties of the matrix can simultaneously affect the biodegradation process of the composites:

(1) The depressed crystallinity of the polymer matrix accelerates the biodegradation process in soil because the amorphous regions are preferred sites for degradation (Eldsäter, Erlandsson, Renstad, Albertsson, & Karlsson, 2000; Guzman et al., 2011).
(2) The high hydrophilicity of the natural fibers promotes the water intake and provide a rougher support for microbial growth (Alvarez et al., 2006).
(3) Huge fiber agglomerates can form micro-cavities promoting the water intake but also drastically diminish the contact surface between the fiber and the polymer diminishing the effect mentioned in Section 2.

It must be also taken into account that the hydrophobic nature of PCL makes it not compatible with hydrophilic fibers, therefore, the fibers with higher hydrophilicity, which are supposed to accelerate the biodegradation process, will also form higher agglomerates when they are blended with PCL favoring the third characteristic. For a better understanding of the difficulty to analyze the soil-burial biodegradation behavior of these materials, it can be noticed that the HCE filler did not substantially change the crystallinity degree of the matrix but, on the other hand, it was the most hydrophilic one and huge agglomerates were seen in the PCL/HCE composites, while the CE and CO fillers lowered the crystallinity degree of the PCL and showed lower hydrophilicity and better dispersion inside the matrix. It is not possible to state which one of these 3 characteristics is controlling the soil-burial behavior of the PCL and their composites but a balance between them is responsible of the results shown in Fig. 7(a and b).

4. Conclusions

The effect of the lignocellulosic filler type and content on the crystallization process and mechanical properties of polycaprolactone based composites has been established. It was determined that the incorporation of a filler clearly influence the crystallization behavior of the pure matrix in terms of the crystallinity degree, the perfection of the crystal, the nucleation sort; the overall crystallization rate and also the model parameters depending on the reinforcement type and content.

The mechanical properties were also influenced for similar parameters than those that affect the crystallization process but unexpected results were obtained. The main reason was that several parameters such as chemical compatibility, interfacial strength, filler dispersion and filler aspect ratio were worsened in the preparation of the high mechanical performance fibers (HCE), therefore they were not useful as reinforcement for PCL.

The tendencies observed for the barrier properties and the biodegradation in soil were a consequence of a balance between the crystallinity degree of the matrix, the PCL/filler chemical compatibility and the dispersion of the filler inside the matrix.

The best performance was obtained with the 15CE composite which showed the highest mechanical properties and did not change the barrier properties of the neat matrix. On the other hand the biodegradation process was accelerated by the presence of these filler but the effect was not severe. Therefore, this material can be useful for packaging applications.

The obtained results demonstrated that the effort and costs involved in the chemical treatments to prepare the HCE filler were not justified; therefore, it is advisable to perform a similar analysis when polymer/HCE composites are studied.

Acknowledgements

Authors acknowledge to Mincyt, UNMdP and CONICET for the financial support.

References

Akil, H. M., Omar, M. F., Mazuki, A. A. M., Safiee, S., Ishak, Z. A. M., & Abu Bakar, A. (2011). Kenaf fiber reinforced composites: a review. *Materials & Design*, *32*(8–9), 4107–4121.

Alvarez, V. A., Ruseckaite, R. A., & Vázquez, A. (2006). Degradation of sisal fibre/mater Bi–Y biocomposites buried in soil. *Polymer Degradation and Stability*, *91*(12), 3156–3162.

Angles, M. N., & Dufresne, A. (2001). Plasticized starch/tunicin whiskers nanocomposite materials. 2. Mechanical behavior. *Macromolecules*, *34*(9), 2921–2931.

Avrami, M. (1939). Kinetics of phase change. I: General theory. *The Journal of Chemical Physics*, *7*(12), 1103–1112.

Azizi Samir, M. A. S., Mateos, A. M., Alloin, F., Sanchez, J.-Y., & Dufresne, A. (2004). Plasticized nanocomposite polymer electrolytes based on poly(oxyethylene) and cellulose whiskers. *Electrochimica Acta*, *49*(26), 4667–4677.

Azizi Samir, M. A. S., Alloin, F., & Dufresne, A. (2005). Review of recent research into cellulosic whiskers, their properties and their application in nanocomposite field. *Biomacromolecules*, *6*(2), 612–626.

Beckermann, G. W., & Pickering, K. L. (2009). Engineering and evaluation of hemp fibre reinforced polypropylene composites: Micro-mechanics and strength prediction modelling. *Composites Part A: Applied Science and Manufacturing*, *40*(2), 210–217.

Belbekhouche, S., Bras, J., Siqueira, G., Chappey, C., Lebrun, L., Khelifi, B., Marais, S., & Dufresne, A. (2011). Water sorption behavior and gas barrier properties of cellulose whiskers and microfibrils films. *Carbohydrate Polymers*, *83*(4), 1740–1748.

Belgacem, M. N., & Gandini, A. (2005). The surface modification of cellulose fibres for use as reinforcing elements in composite materials. *Composite Interfaces*, *12*(1), 41–75.

Bessadok, A., Langevin, D., Gouanvé, F., Chappey, C., Roudesli, S., & Marais, S. (2009). Study of water sorption on modified Agave fibres. *Carbohydrate Polymers*, *76*(1), 74–85.

Bledzki, A. K., & Gassan, J. (1999). Composites reinforced with cellulose based fibres. *Progress in Polymer Science*, *24*(2), 221–274.

Bourmaud, A., & Pimbert, S. (2008). Investigations on mechanical properties of poly(propylene) and poly(lactic acid) reinforced by miscanthus fibers. *Composites Part A: Applied Science and Manufacturing*, *39*(9), 1444–1454.

Brahim, S. B., & Cheikh, R. B. (2007). Influence of fibre orientation and volume fraction on the tensile properties of unidirectional Alfa-polyester composite. *Composites Science and Technology*, *67*(1), 140–147.

Cai, Y., Petermann, J., & Wittich, H. (1997). Transcrystallization in fiber-reinforced isotactic polypropylene composites in a temperature gradient. *Journal of Applied Polymer Science*, *65*(1), 67–75.

Chen, Y., Liu, C., Chang, P. R., Cao, X., & Anderson, D. P. (2009). Bionanocomposites based on pea starch and cellulose nanowhiskers hydrolyzed from pea hull fibre: Effect of hydrolysis time. *Carbohydrate Polymers*, *76*(4), 607–615.

Cyras, V. P., Vázquez, A., & Kenny, J. M. (2001). Crystallization kinetics by differential scanning calorimetry for PCL/starch and their reinforced sisal fiber composites. *Polymer Engineering & Science*, *41*(9), 1521–1528.

de Morais, A. B. (2006). Prediction of the longitudinal tensile strength of polymer matrix composites. *Composites Science and Technology*, *66*(15), 2990–2996.

Desio, G. P., & Rebenfeld, L. (1992). Crystallization of fiber-reinforced poly(phenylene sulfide) composites. II. Modeling the crystallization kinetics. *Journal of Applied Polymer Science*, *45*(11), 2005–2020.

Di Franco, C. R., Cyras, V. P., Busalmen, J. P., Ruseckaite, R. A., & Vázquez, A. (2004). Degradation of polycaprolactone/starch blends and composites with sisal fibre. *Polymer Degradation and Stability*, *86*(1), 95–103.

Dubois, P., Jacobs, C., Jerome, R., & Teyssie, P. (1991). Macromolecular engineering of polylactones and polylactides. 4. Mechanism and kinetics of lactide homopolymerization by aluminum isopropoxide. *Macromolecules*, *24*(9), 2266–2270.

Dufresne, A. (2006). Comparing the mechanical properties of high performances polymer nanocomposites from biological sources. *Journal of Nanoscience and Nanotechnology*, *6*(2), 322–330.

Dufresne, A., Dupeyre, D., & Vignon, M. R. (2000). Cellulose microfibrils from potato tuber cells: Processing and characterization of starch-cellulose microfibril composites. *Journal of Applied Polymer Science*, *76*(14), 2080–2092.

Eichhorn, S. J., Baillie, C. A., Zafeiropoulos, N., Mwaikambo, L. Y., Ansell, M. P., Dufresne, A., et al. (2001). Review: Current international research into cellulosic fibres and composites. *Journal of Materials Science*, *36*(9), 2107–2131.

Eldsäter, C., Erlandsson, B., Renstad, R., Albertsson, A. C., & Karlsson, S. (2000). The biodegradation of amorphous and crystalline regions in film-blown poly([epsilon]-caprolactone). *Polymer*, *41*(4), 1297–1304.

El-Tayeb, N. S. M. (2009). Development and characterisation of low-cost polymeric composite materials. *Materials & Design*, *30*(4), 1151–1160.

Freire, C. S. R., Silvestre, A. J. D., Pascoal Neto, C., Belgacem, M. N., & Gandini, A. (2006). Controlled heterogeneous modification of cellulose fibers with fatty acids: Effect of reaction conditions on the extent of esterification and fiber properties. *Journal of Applied Polymer Science*, *100*(2), 1093–1102.

Gorrasi, G., Tortora, M., Vittoria, V., Pollet, E., Lepoittevin, B., Alexandre, M., & Dubois, P. (2003). Vapor barrier properties of polycaprolactone montmorillonite nanocomposites: Effect of clay dispersion. *Polymer*, *44*(8), 2271–2279.

Gray, D. G., & Guillet, J. E. (1974). Open tubular columns for studies on polymer stationary phases by gas chromatography. *Journal of Polymer Science: Polymer Letters Edition*, *12*(4), 231–235.

Grima, S., Bellon-Maurel, V., Feuilloley, P., & Silvestre, F. (2000). Aerobic biodegradation of polymers in solid-state conditions: A review of environmental and physicochemical parameter settings in laboratory simulations. *Journal of Polymers and the Environment*, *8*(4), 183–195.

Guzman, A., Gnutek, N., & Janik, H. (2011). Biodegradable polymers for food packaging—Factors influencing their degradation and certification types—A comprehensive review. *Chemistry & Chemical Technology*, *5*(1), p7.

Hablot, E., Matadi, R., Ahzi, S., & Avérous, L. (2010). Renewable biocomposites of dimer fatty acid-based polyamides with cellulose fibres: Thermal, physical and mechanical properties. *Composites Science and Technology*, *70*(3), 504–509.

Huda, M. S., Drzal, L. T., Misra, M., Mohanty, A. K., Williams, K., & Mielewski, D. F. (2005). A study on biocomposites from recycled newspaper fiber and poly(lactic acid). *Industrial & Engineering Chemistry Research*, *44*(15), 5593–5601.

Huson, M. G., & McGill, W. J. (1984). Transcrystallinity in polypropylene. *Journal of Polymer Science: Polymer Chemistry Edition*, *22*(11), 3571–3580.

Joseph, P. V., Joseph, K., Thomas, S., Pillai, C. K. S., Prasad, V. S., Groeninckx, G., et al. (2003). The thermal and crystallisation studies of short sisal fibre reinforced polypropylene composites. *Composites Part A: Applied Science and Manufacturing*, *34*(3), 253–266.

Kim, E. G., Kim, B. S., & Kim, D. S. (2007). Physical properties and morphology of polycaprolactone/starch/pine-leaf composites. *Journal of Applied Polymer Science*, *103*(2), 928–934.

Krikorian, V., & Pochan, D. J. (2004). Unusual crystallization behavior of organoclay reinforced poly(L-lactic acid) nanocomposites. *Macromolecules*, *37*(17), 6480–6491.

Ku, H., Wang, H., Pattarachaiyakoop, N., & Trada, M. (2011). A review on the tensile properties of natural fiber reinforced polymer composites. *Composites Part B: Engineering*, *42*(4), 856–873.

Kunioka, M., Ninomiya, F., & Funabashi, M. (2007). Novel evaluation method of biodegradabilities for oil-based polycaprolactone by naturally occurring radiocarbon-14 concentration using accelerator mass spectrometry based on ISO 14855-2 in controlled compost. *Polymer Degradation and Stability*, *92*(7), 1279–1288.

Lepoittevin, B., Devalckenaere, M., Pantoustier, N., Alexandre, M., Kubies, D., Calberg, C., et al. (2002). Poly([var epsilon]-caprolactone)/clay nanocomposites prepared by melt intercalation: Mechanical, thermal and rheological properties. *Polymer*, *43*(14), 4017–4023.

Lin, C. W., Ding, S. Y., & Hwang, Y. W. (2001). Interfacial crystallization of isotactic polypropylene molded against the copper surface with various surface roughnesses prepared by an electrochemical process. *Journal of Materials Science*, *36*(20), 4943–4948.

Lönnberg, H., Fogelström, L., Berglund, L., Malmström, E., & Hult, A. (2008). Surface grafting of microfibrillated cellulose with poly([epsilon]-caprolactone)—Synthesis and characterization. *European Polymer Journal*, *44*(9), 2991–2997.

Ludueña, L. N., Alvarez, V. A., & Vazquez, A. (2007). Processing and microstructure of PCL/clay nanocomposites. *Materials Science and Engineering A*, *460–461*, 121–129.

Ma, X., Yu, J., & Kennedy, J. F. (2005). Studies on the properties of natural fibers-reinforced thermoplastic starch composites. *Carbohydrate Polymers*, *62*(1), 19–24.

Morán, J., Alvarez, V., Cyras, V., & Vázquez, A. (2008). Extraction of cellulose and preparation of nanocellulose from sisal fibers. *Cellulose*, *15*(1), 149–159.

Morin, A., & Dufresne, A. (2002). Nanocomposites of chitin whiskers from Riftia tubes and poly(caprolactone). *Macromolecules*, *35*(6), 2190–2199.

Mwaikambo, L. Y., & Ansell, M. P. (2002). Chemical modification of hemp, sisal, jute, and kapok fibers by alkalization. *Journal of Applied Polymer Science*, *84*(12), 2222–2234.

Nishino, T. (2004). Green composites: polymer composites and the environment. In C. Baillie (Ed.), *Abington Hall, Abington Cambridge, England* (pp. 49–80). Woodhead publishing limited.

Oh, S. Y., Yoo, D. I., Shin, Y., & Seo, G. (2005). FTIR analysis of cellulose treated with sodium hydroxide and carbon dioxide. *Carbohydrate Research*, *340*(3), 417–428.

Oksman, K., Skrifvars, M., & Selin, J. F. (2003). Natural fibres as reinforcement in polylactic acid (PLA) composites. *Composites Science and Technology*, *63*(9), 1317–1324.

Orts, W. J., Shey, J., Imam, S. H., Glenn, G. M., Guttman, M. E., & Revol, J.-F. (2005). Application of cellulose microfibrils in polymer nanocomposites. *Journal of Polymers and the Environment*, *13*(4), 301–306.

Peneva, Y., & Minkova, L. (2006). Non-isothermal and isothermal crystallization of nanocomposites based on functionalized polyethylenes. *Polymer Testing*, *25*(3), 366–376.

Pérez, C., Alvarez, V., Stefani, P., & Vázquez, A. (2007). Non-isothermal crystallization of MaterBi-Z/clay nanocomposites. *Journal of Thermal Analysis and Calorimetry*, *88*(3), 825–832.

Petersen, K., Væggemose Nielsen, P., Bertelsen, G., Lawther, M., Olsen, M. B., Nilsson, N. H., et al. (1999). Potential of biobased materials for food packaging. *Trends in Food Science & Technology*, *10*(2), 52–68.

Petersson, L., & Oksman, K. (2006). Biopolymer based nanocomposites: Comparing layered silicates and microcrystalline cellulose as nanoreinforcement. *Composites Science and Technology*, *66*(13), 2187–2196.

Quan, H., Li, Z.-M., Yang, M.-B., & Huang, R. (2005). On transcrystallinity in semi-crystalline polymer composites. *Composites Science and Technology*, *65*(7–8), 999–1021.

Reinsch, V. E., & Rebenfeld, L. (1994). Crystallization processes in poly(ethylene terephthalate) as modified by polymer additives and fiber reinforcement. *Journal of Applied Polymer Science*, *52*(5), 649–662.

Roman, M., & Winter, W. T. (2004). Effect of sulfate groups from sulfuric acid hydrolysis on the thermal degradation behavior of bacterial cellulose. *Biomacromolecules*, *5*(5), 1671–1677.

Rosa, M. F., Medeiros, E. S., Malmonge, J. A., Gregorski, K. S., Wood, D. F., Mattoso, L. H. C., et al. (2010). Cellulose nanowhiskers from coconut husk fibers: Effect of preparation conditions on their thermal and morphological behavior. *Carbohydrate Polymers*, *81*(1), 83–92.

Sanchez-Garcia, M. D., Gimenez, E., & Lagaron, J. M. (2008). Morphology and barrier properties of solvent cast composites of thermoplastic biopolymers and purified cellulose fibers. *Carbohydrate Polymers*, *71*(2), 235–244.

Singh, S., Mohanty, A. K., Sugie, T., Takai, Y., & Hamada, H. (2008). Renewable resource based biocomposites from natural fiber and polyhydroxybutyrate-co-valerate (PHBV) bioplastic. *Composites Part A: Applied Science and Manufacturing*, *39*(5), 875–886.

Siró, I., & Plackett, D. (2010). Microfibrillated cellulose and new nanocomposite materials: A review. *Cellulose*, *17*(3), 459–494.

Son, S.-J., Lee, Y.-M., & Im, S.-S. (2000). Transcrystalline morphology and mechanical properties in polypropylene composites containing cellulose treated with sodium hydroxide and cellulase. *Journal of Materials Science*, *35*(22), 5767–5778.

Strawhecker, K. E., & Manias, E. (2003). Crystallization behavior of poly(ethylene oxide) in the presence of Na^+ montmorillonite fillers. *Chemistry of Materials*, *15*(4), 844–849.

Swapna Joseph, C., Harish Prashanth, K., Rastogi, N., Indiramma, A., Yella Reddy, S., & Raghavarao, K. (2009). Optimum blend of chitosan and poly-(ε-caprolactone) for fabrication of films for food packaging applications. *Food and Bioprocess Technology*, 1–7.

Wang, C., & Liu, C. R. (1999). Transcrystallization of polypropylene composites: Nucleating ability of fibres. *Polymer*, *40*(2), 289–298.

Wang, N., Ding, E., & Cheng, R. (2007). Thermal degradation behaviors of spherical cellulose nanocrystals with sulfate groups. *Polymer*, *48*(12), 3486–3493.

Wollerdorfer, M., & Bader, H. (1998). Influence of natural fibres on the mechanical properties of biodegradable polymers. *Industrial Crops and Products*, *8*(2), 105–112.

Wu, T.-M., & Liu, C.-Y. (2005). Poly(ethylene 2,6-naphthalate)/layered silicate nanocomposites: Fabrication, crystallization behavior and properties. *Polymer*, *46*(15), 5621–5629.

Yam, W. Y., Ismail, J., Kammer, H. W., Schmidt, H., & Kummerlöwe, C. (1999). Polymer blends of poly([epsilon]-caprolactone) and poly(vinyl methyl ether)—Thermal properties and morphology. *Polymer*, *40*(20), 5545–5552.

Yang, H., Yan, R., Chen, H., Lee, D. H., & Zheng, C. (2007). Characteristics of hemicellulose, cellulose and lignin pyrolysis. *Fuel*, *86*(12–13), 1781–1788.

Yu, L., Dean, K., & Li, L. (2006). Polymer blends and composites from renewable resources. *Progress in Polymer Science*, *31*(6), 576–602.

Yue, C. Y., & Cheung, W. L. (1993). Some observations on the role of transcrystalline interphase on the interfacial strength of thermoplastic composites. *Journal of Materials Science Letters*, *12*(14), 1092–1094.

Zhao, Q., Tao, J., Yam, R. C. M., Mok, A. C. K., Li, R. K. Y., & Song, C. (2008). Biodegradation behavior of polycaprolactone/rice husk ecocomposites in simulated soil medium. *Polymer Degradation and Stability*, *93*(8), 1571–1576.